RESEARCH BRIEF

Ectopic Humanized Mesenchymal Niche in Mice Enables Robust Engraftment of Myelodysplastic Stem Cells

Syed A. Mian[1,2], Ander Abarrategi[2], Kar Lok Kong[1], Kevin Rouault-Pierre[2], Henry Wood[1,3], Caroline A. Oedekoven[2], Alexander E. Smith[1,3], Antoniana Batsivari[2], Linda Ariza-McNaughton[2], Peter Johnson[4], Thomas Snoeks[4], Ghulam J. Mufti[1,3], and Dominique Bonnet[2]

ABSTRACT

Myelodysplastic syndromes (MDS) are clonal stem cell diseases characterized mainly by ineffective hematopoiesis. Here, we present an approach that enables robust long-term engraftment of primary MDS stem cells (MDS-SC) in mice by implantation of human mesenchymal cell–seeded scaffolds. Critically for modeling MDS, where patient sample material is limiting, mononuclear bone marrow cells containing as few as 10^4 $CD34^+$ cells can be engrafted and expanded by this approach with the maintenance of the genetic make-up seen in the patients. Noninvasive high-resolution ultrasound imaging shows that these scaffolds are fully perfused. Our data show that the human microenvironment but not mouse is essential to MDS-SC homing and engraftment. Notably, the alternative niche provided by healthy donor mesenchymal stromal cells enhances engraftment of MDS-SCs. This study characterizes a new tool to model MDS human disease with the level of engraftment previously unattainable in mice and offers insights into human-specific determinants of the MDS-SC microenvironment.

SIGNIFICANCE: These findings are significant for understanding the niche dependence of MDS. This report provides the evidence of the migratory behavior of hematopoietic stem cells in myeloid cancers. Our model offers a unique opportunity to study the clonal behavior of the myeloid/lymphoid cancers and delineate how cancer cells interact with different niches.

[1]Department of Haematology, School of Cancer and Pharmaceutical Sciences, King's College London, London, United Kingdom. [2]Haematopoietic Stem Cell Lab, The Francis Crick Institute, London, United Kingdom. [3]King's College Hospital London, London, United Kingdom. [4]Imaging Research Facility, The Francis Crick Institute, London, United Kingdom.

Note: Supplementary data for this article are available at Blood Cancer Discovery Online (https://bloodcancerdiscov.aacrjournals.org/).

G.J. Mufti and D. Bonnet contributed equally to this article.

Current address for A. Abarrategi: Regenerative Medicine Laboratory, Center for Cooperative Research in Biomaterials (CIC biomaGUNE), Basque Research and Technology Alliance (BRTA), Basque Foundation for Science (Ikerbasque), Donostia San Sebastián, Spain; and current address for K. Rouault-Pierre, Centre for Haemato-Oncology, Barts Cancer Institute, Queen Mary University of London, London, United Kingdom.

Corresponding Authors: Dominique Bonnet, The Francis Crick Institute, 1 Midland Road, London NW1A 1AT, UK. Phone: 44 (0) 2037961198; E-mail: dominique.bonnet@crick.ac.uk; and Ghulam J. Mufti, Department of Haematology, School of Cancer and Pharmaceutical Sciences, King's College London, London, UK. Phone: 44 (0) 2032993080; E-mail: ghulam.mufti@kcl.ac.uk

Blood Cancer Discov 2021;2:135–45

doi: 10.1158/2643-3230.BCD-20-0161

INTRODUCTION

Myelodysplastic syndromes (MDS) are a group of hematopoietic stem cell (HSC) disorders (1, 2), with a high propensity to transform to acute myeloid leukemia (AML). In a spectrum of myeloid disorders ranging from age-related clonal hematopoiesis (ARCH) to AML, MDS is mainly distinguished by the presence of peripheral blood cytopenias, dysplastic hematopoietic differentiation, and the lack of features that define acute leukemia. MDS disease is driven by a complex combination of somatic gene mutations and/or chromosomal abnormalities, particularly targeting the myeloid lineage (3–6).

Understanding the biology of MDS stem cells (MDS-SC) and decoding their interaction with the bone marrow (BM) microenvironment remain major challenges due to the lack of reliable *in vivo* disease models, therefore impeding translational MDS research. Attempts to generate and use humanized transgenic mice have provided limited improvement in generating xenograft models for MDS (7, 8). Although coinjection of mesenchymal stromal cells (MSC) along with MDS CD34$^+$ cells into the murine BM was initially suggested to help MDS engraftment in patient-derived xenograft (PDX) models (7), subsequent studies showed no beneficial effect (8, 9). These efforts to construct a model that replicates the cellular human BM niche have been limited until now, as they have been based on simple injection of MDS hematopoietic stem and progenitor cells (HSPC) into murine hematopoietic tissue. This has also restricted our ability to map the specific interactions that may exist in the human BM microenvironment (10–12). Being able to study these interactions in more physiologic humanized conditions is essential as it will allow us to better understand the intercellular signaling that we anticipate may be critical in the initiation, maintenance, and progression of MDS. Recent advances in bioengineering have enabled the integration of novel biomaterials into developmental biology. These biomaterials provide a versatile tool to create a humanized microenvironment in immunodeficient mouse models (13). These "special niches" are invaluable for providing architectural support for cell attachment, cellular differentiation, and tissue development, therefore enabling key cell–cell biological interactions.

RESULTS

MDS BM Stem Cells Robustly Engraft in *In Vivo* Three-dimensional Humanized Scaffolds

PDX mouse models have proven their reliability in recapitulating features of malignant hematopoiesis, particularly in acute leukemia (13–17). However, attempts to recapitulate this success in other more chronic hematopoietic malignancies such as MDS have yielded little or no success (3, 6, 8–12). This prompted us to develop an alternative *in vivo* system that enables rapid and reliable assessment of the HSPCs. This xenotransplantation system uses gelatin-based porous scaffolds (hereafter defined as humanized scaffolds) to generate niches in mice that mimic the human-specific microenvironment.

Our study is based on 37 patients [MDS with multilineage dysplasia (MDS-MLD) = 20, MDS with excess blasts (MDS-EB) = 4, MDS, unclassifiable (MDS-U) = 2, MDS with single lineage dysplasia with ring sideroblasts (MDS-SLD-RS) = 3, MDS-MLD with ring sideroblasts (MDS-MLD-RS) = 4, chronic myelomonocytic leukemia (CMML) = 2, MDS/myeloproliferative neoplasia (MPN) = 1, and secondary AML (sAML) = 1; Supplementary Tables S1–S3] and healthy donors (n = 6). Whole-exome sequencing (WES) or myeloid-specific gene panel screening demonstrated a mutational distribution (Supplementary Fig. S1A) as previously reported (4, 5). BM MSCs from patients with MDS isolated for use in the *in vivo* experiments showed variable expansion levels consistent with previous reports (18).

Initially, we chose to screen five patients in NSG and NSG-SGM3 mice by injecting BM CD3-depleted mononuclear cells (MNC, hereafter defined as HSPCs; 0.25×10^6 to 0.75×10^6) into scaffolds that were preseeded with autologous (or allogenic MDS MSCs, where autologous MSCs were not available) patient-derived MSCs (Fig. 1A) and s.c. transplanted in mice. Humanized scaffold tissues recovered 12 to 18 weeks after implantation showed uniform distribution of human CD45$^+$ (hCD45$^+$) cells throughout the scaffold as well as the presence of murine vasculature, with hCD45$^+$ cells present adjacent to the murine vascular structures within the humanized scaffolds. In addition, murine CD45$^+$ cells were also observed in these humanized scaffolds but relatively fewer in number (Fig. 1B and C; Supplementary Fig. S1B). These humanized scaffolds act as a framework to support cell proliferation and differentiation, and maintain not only the primary cellular phenotype and function but also the dysplastic morphology (Fig. 1B, right; Supplementary Fig. S1C) typically observed in MDS BM and blood. Although there was no significant difference in the hCD45$^+$ cell engraftment between NSG and NSG-SGM3 mice (Fig. 1D), humanized scaffolds harvested from the NSG-SGM3 mice appeared larger compared with the ones obtained from NSG mice (Supplementary Fig. S1D), and the recovery of human myeloid cells (CD45$^+$CD33$^+$) was significantly higher from NSG-SGM3 mice (Fig. 1E). We did not observe any significant increase in the engraftment levels in the humanized scaffolds when mice were kept alive for up to 24 weeks (NSG-SGM3 12-week median hCD45$^+$ cells = 10.6%, 24-week hCD45$^+$ cells = 4.4%; P value = 0.1; Supplementary Fig. S1E). We therefore opted to use our three-dimensional (3D) humanized scaffold system in NSG-SGM3 mice to study an additional cohort of patients with MDS, covering a range of MDS risk groups and closely related myeloid malignancies (Supplementary Table S2). We observed persistent long-term engraftment of hCD45$^+$ cells within the humanized scaffolds ranging from 0.2% to 86%, with 82% of cases having ≥20% hCD45$^+$ cells (Fig. 2A). There was no significant difference in the engraftment levels between low-risk cases (mean hCD45$^+$ cells, MDS-U = 35.5%, MDS-SLD = 22.5%, MDS-MLD-RS = 30.4%, MDS-MLD = 30.7%) and high-risk MDS cases (mean hCD45$^+$ cells, MDS-EB = 21.88%; Fig. 2A and B). In some cases, such as patients 23 and 31, the average engraftment of MDS cells was low (hCD45$^+$ cells <1%). The humanized scaffolds in these mice showed multilineage engraftment of human hematopoiesis. Notably, mice that received HSPCs from MDS-EB cases had higher myeloid lineage engraftment compared with low-risk MDS cases (MDS-SLD-RS hCD33$^+$ = 44%; MDS-MLD hCD33$^+$ = 46.6%; MDS-EB hCD33$^+$ = 65%; Fig. 2C). Similarly,

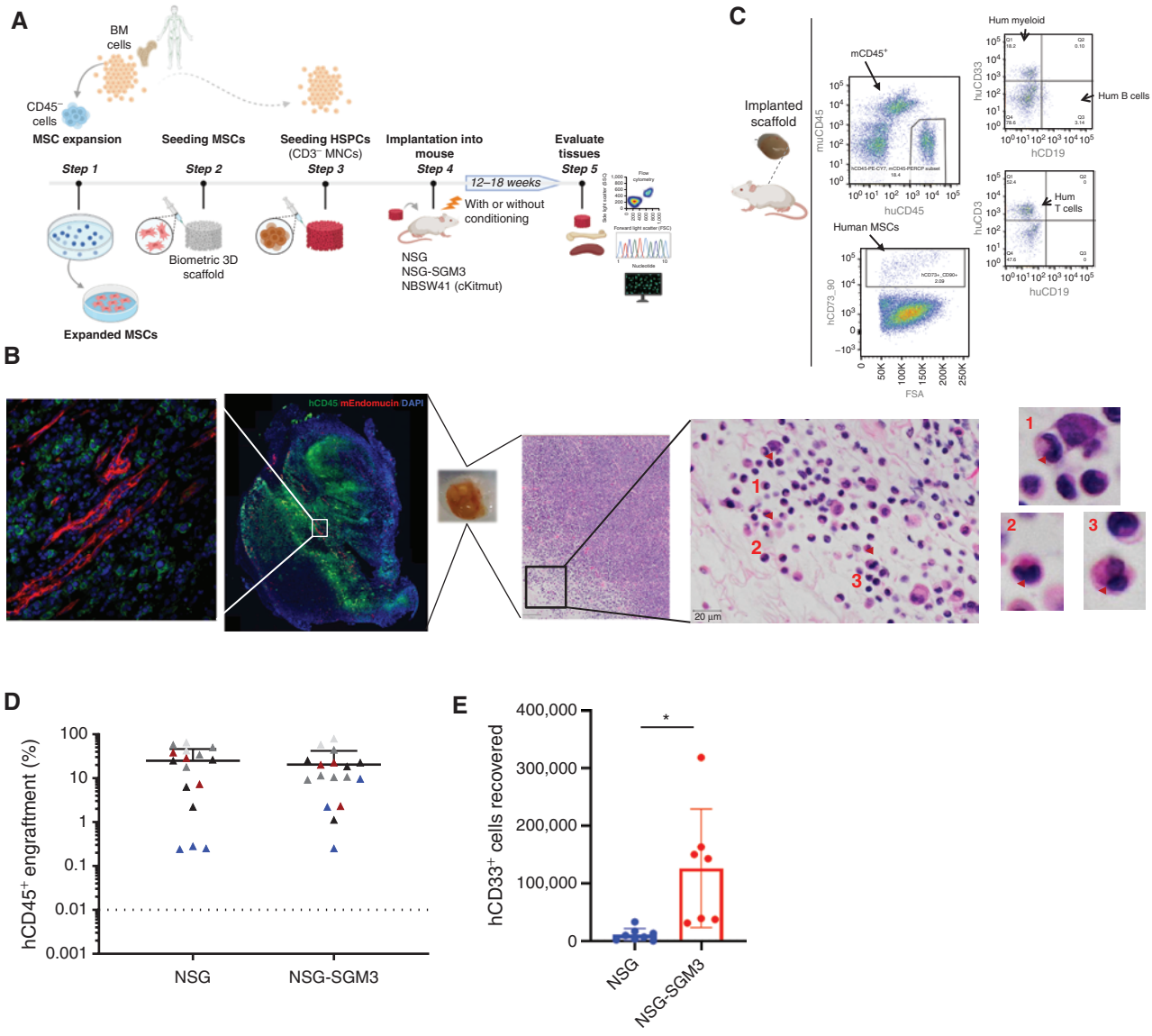

Figure 1. Humanized scaffold system in NSG and NSG-SGM3 immunodeficient mice. **A,** Schematic representation of the *in vivo* protocol used for generating humanized scaffolds. Illustration was created with BioRender.com. **B,** Representative example of immunofluorescence and hematoxylin and eosin (H&E) staining for the scaffold retrieved following the xenotransplantation. H&E staining of a section of the engrafted scaffold shows multiple neutrophils with hypolobated nuclei (examples indicated with arrowheads), consistent with dysplasia in the granulocytic lineage. **C,** Representative flow cytometry plot of the cells retrieved from the humanized scaffolds following xenotransplantation. **D,** Comparison of hCD45⁺ cells engraftment in humanized scaffolds retrieved from NSG and NSG-SGM3 mice 12 weeks following the scaffold implantation. **E,** Absolute cell counts of human myeloid (hCD45⁺hCD33⁺) cells retrieved from humanized scaffolds implanted in NSG and NSG-SGM3 mice. *, $P \leq 0.05$.

myeloid bias was also observed in mice transplanted with MDS/MPN, CMML, and sAML BM HSPCs. Taken together, our data provide a reliable *in vivo* model system that can be used to robustly engraft MDS HSPCs in preclinical studies.

HSPCs carrying MDS-associated gene mutations constitute a reservoir of preleukemic stem cells (3, 5, 6) that undergo evolution acquiring additional mutations, leading to transformation to AML. We used DNA molecular testing to compare the mutations present in the engrafted cells harvested from the humanized scaffolds in the mice with those that were initially identified in the patients' primary BM HSPCs (Supplementary Table S3). Patient-specific targeted mutation screening was performed on the harvested hCD45⁺hCD33⁺ cells by next-generation MiSeq sequencing. Our analysis showed that in the implanted humanized scaffolds, variant allele frequency of the mutations was largely maintained in both NSG and NSG-SGM3 mouse models (Fig. 2D; Supplementary Fig. S2; Supplementary Table S4). Interestingly, mutations that have been previously described as disease initiating, such as *SF3B1, DNMT3A, SRSF2*, and *TET2*, as well as those associated with disease progression, such as *ASXL1, NRAS*, and *RUNX1*, were all maintained in the humanized scaffolds in all the cases, indicating that these humanized niches in mice maintain the original clonal MDS architecture.

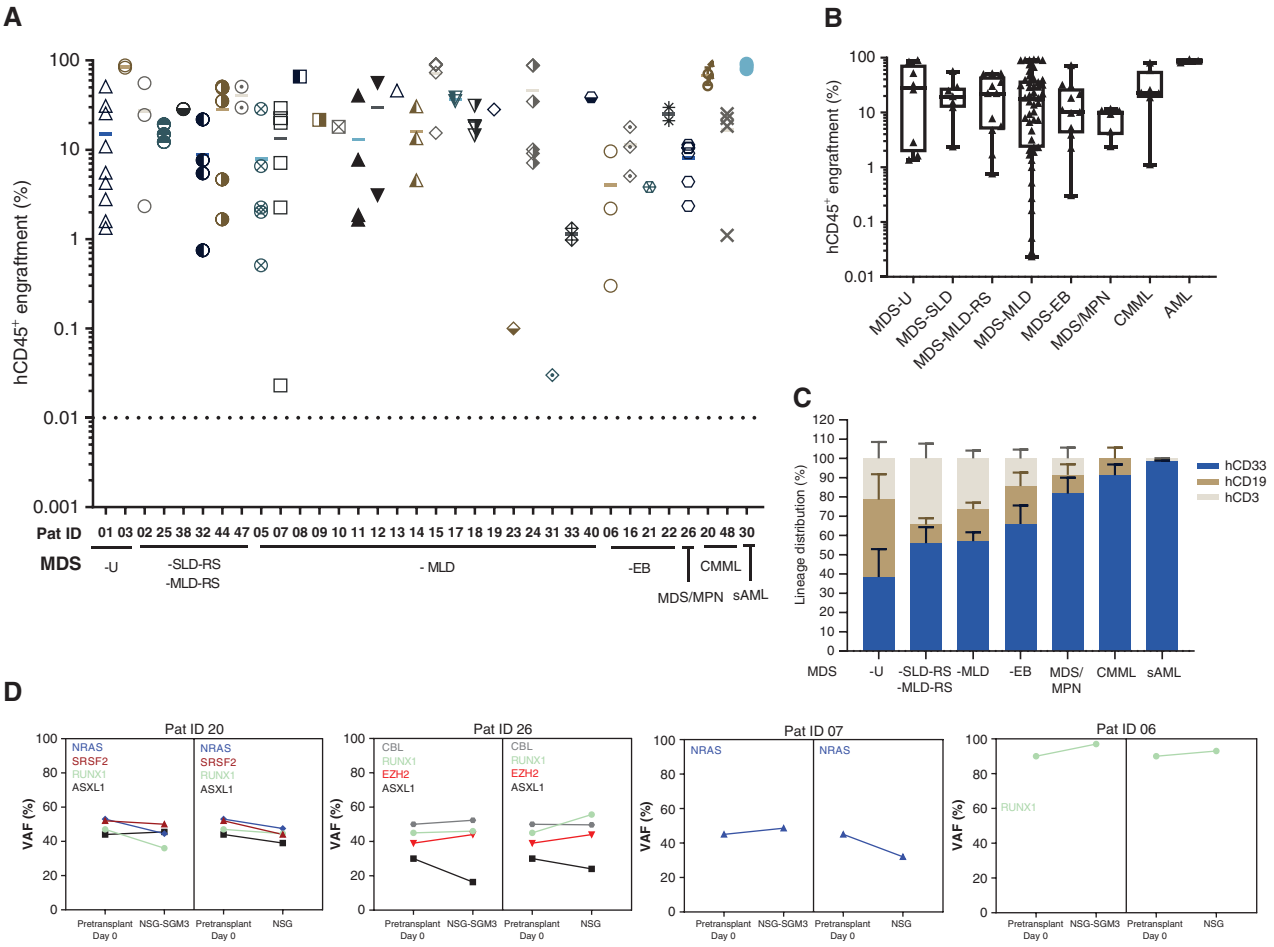

Figure 2. Humanized niches in immunodeficient mice enable the robust engraftment of MDS HSPCs. **A,** Total hCD45+ cell engraftment in humanized scaffolds implanted in NSG-SGM3 mice. Mice were kept alive for up to 18 weeks following the scaffold implantation. Pat ID, patient ID. **B,** Comparison of total hCD45+ cell engraftment in humanized scaffolds following xenotransplantation in various MDS World Health Organization (WHO) subtypes and other related myeloid malignancies. **C,** Lineage distribution within the hCD45+ cells recovered from the humanized scaffolds implanted in NSG-SGM3 mice. **D,** Mutational spectrum of the MDS HSPCs in primary pretransplanted cells and posttransplanted cells from humanized MDS scaffolds in NSG and NSG-SGM3 mice. Variant allele frequency (VAF) for xenografted samples is the average between two and three mice (where applicable).

Humanized Scaffolds Enable the Maintenance of Long-term Self-renewal Capacity of MDS-SCs

Long-term self-renewal ability has been traditionally used to define stemness of HSCs. We first sought to determine if the humanized niches implanted in the immunodeficient mice were able to maintain the long-term MDS-SCs. MDS $CD34^+CD38^-$ stem cells were flow sorted, seeded into the humanized niches, and then transplanted into the NSG-SGM3 mice. Even though we transplanted a variable number of $CD34^+CD38^-$ stem cells (range, 1,300–11,000 $CD34^+CD38^-$), engraftment of these MDS-SCs was observed in all cases (Fig. 3A–C). Interestingly, MDS $CD34^+$ HSPCs were detected at a high frequency in $CD34^+CD38^-$-injected mice (mean $hCD34^+CD38^-$ = 35.24%; $hCD34^+CD38^+$ = 36.26) than in BM MNC $CD3^-$–injected mice (mean $hCD34^+$ = 6.1%) in primary transplants, even up to 18 weeks after xenotransplantation (Fig. 3C and D). In addition, $CD34^+CD38^-$ also differentiated to mature progeny ($CD34^+C38^+$) within these humanized scaffolds.

Next, we tested whether the MDS-SCs present in the humanized scaffolds in the primary mice had self-renewal capacity by performing secondary transplantation assays. Following the primary xenotransplantation, $hCD45^+CD3^-$ cells were isolated by FACS from mice previously engrafted with MDS BM $CD3^-$ cells (Fig. 3E). Four patients were used for serial transplantation. Variable numbers of $hCD45^+CD3^-$ cells were transplanted into the 3D scaffolds in the mice (Supplementary Table S5). Twelve weeks following xenotransplantation in the secondary recipients, all mice demonstrated human cell engraftment in the humanized niches (Fig. 3F). For patient 26, engraftment in the secondary recipient ($hCD45^+$ = 10%) was similar to that observed in the primary transplants. However, for the other three patients, all high engrafters in the primary transplant settings, we observed $hCD45^+$ cell engraftment levels between 0.1% and 1.5% in the secondary recipients. Furthermore, even though T-cell–depleted ($hCD45^+CD3^-$) MDS HSPCs were injected into the secondary recipients, we observed mixed lineage engraftment in two out of four cases (Fig. 3G). Patients 18 and 26 displayed exclusive myeloid lineage engraftment in the secondary recipients. Although the engraftment in some secondary recipients was relatively reduced compared with the

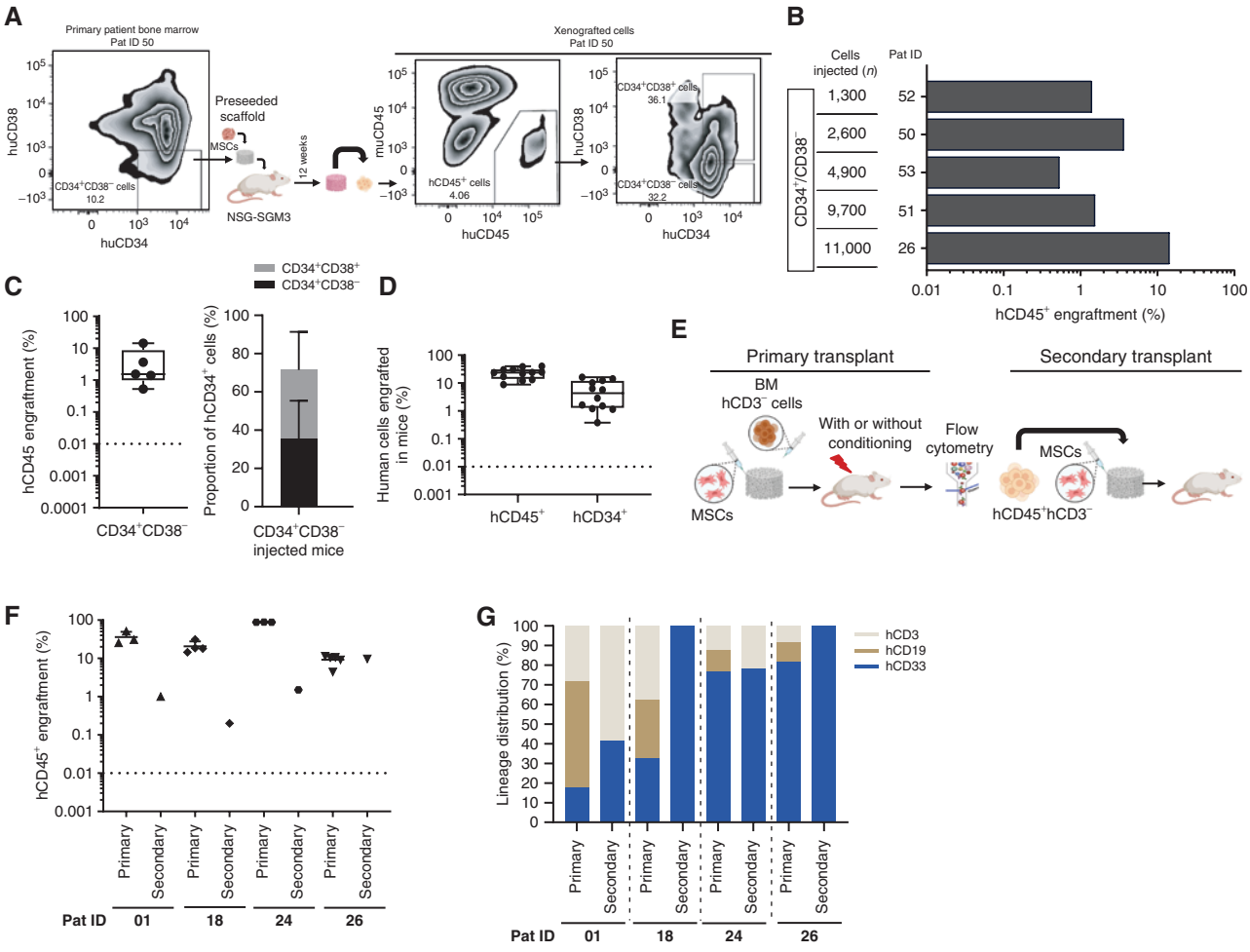

Figure 3. MDS-SCs engraft in humanized niches in NSG-SGM3 mice and demonstrate long-term self-renewal capacity. **A,** Representative flow cytometry plot showing the day 0 patient BM CD34/CD38 phenotype and engraftment of hCD45$^+$ cells in humanized scaffolds as well as the hCD34/hCD38 phenotype of these xenografted cells in NSG-SGM3 mice. Pat ID, patient ID. **B,** Total hCD45$^+$ cell engraftment in humanized scaffolds that were seeded with CD34$^+$CD38$^-$ MDS-SCs in NSG-SGM3 mice. **C,** Percentage of hCD45$^+$ cells (left) in mice injected with CD34$^+$CD38$^-$ MDS cells and proportion of CD34$^+$C38$^-$/CD34$^+$CD38$^+$ cells within hCD34$^+$ HSPCs in these humanized scaffolds retrieved from NSG-SGM3 mice. **D,** Percentage of hCD45$^+$ cells and proportion of hCD34$^+$ cells within the hCD45$^+$ cell fraction in the humanized scaffolds that were seeded with MDS CD3$^-$ MNCs. **E,** Schematic representation of the *in vivo* protocol for secondary transplantation. **F,** Percentage of total hCD45$^+$ cells engrafted in humanized niches from primary and secondary NSG-SGM3 mice. **G,** Lineage distribution within the hCD45$^+$ cells in humanized niches implanted in primary and secondary NSG-SGM3 mice. Mice were kept alive for up to 18 weeks following the scaffold implantation.

corresponding primary transplants, this could be due to the intrinsic aging of the BM HSCs, as similar results have also been observed in normal-aged mouse HSCs elsewhere (19, 20), but also clearly depends on patient samples. Therefore, our data demonstrate that irrespective of the disease risk group and the genomic mutational architecture, the humanized scaffold *in vivo* system can support long-term self-renewal activity of the malignant MDS-SCs.

MDS HSPCs Are Highly Dependent on Humanized Niches

Previous studies have shown that BM HSPCs from patients with MDS can engraft in the immunodeficient murine BM microenvironment (3, 8, 9), albeit at a low level. Therefore, we wanted to determine if MDS HSPCs engrafted in the humanized niches could colonize the murine BM microenvironment. In the majority of the cases, MDS HSPCs were not detected in the BM of sublethally irradiated NSG or NSG-SGM3 mice (Supplementary Fig. S3A). Only three mice had low levels of hCD45$^+$ cells engrafted in the BM. To determine whether the humanized scaffolds had sufficiently perfused vasculature to allow migration of human HSPCs to the mouse BM, we next assessed the perfusion of the scaffolds by high-resolution ultrasound imaging of live mice following injection of microbubbles via the tail vein. The flow of the microbubbles through the mouse vasculature system demonstrated that these humanized scaffolds are fully perfused (Supplementary Video S1). The photoacoustic imaging of biological tissue–engineered scaffolds in live mice provides a novel and promising noninvasive and nondestructive method for assessing vascular and endothelial alterations that have been previously associated with myeloid malignancies, particularly AML (21).

These data prompted us to use a more permissive mouse model (NSGW41; ref. 22) where the endogenous murine

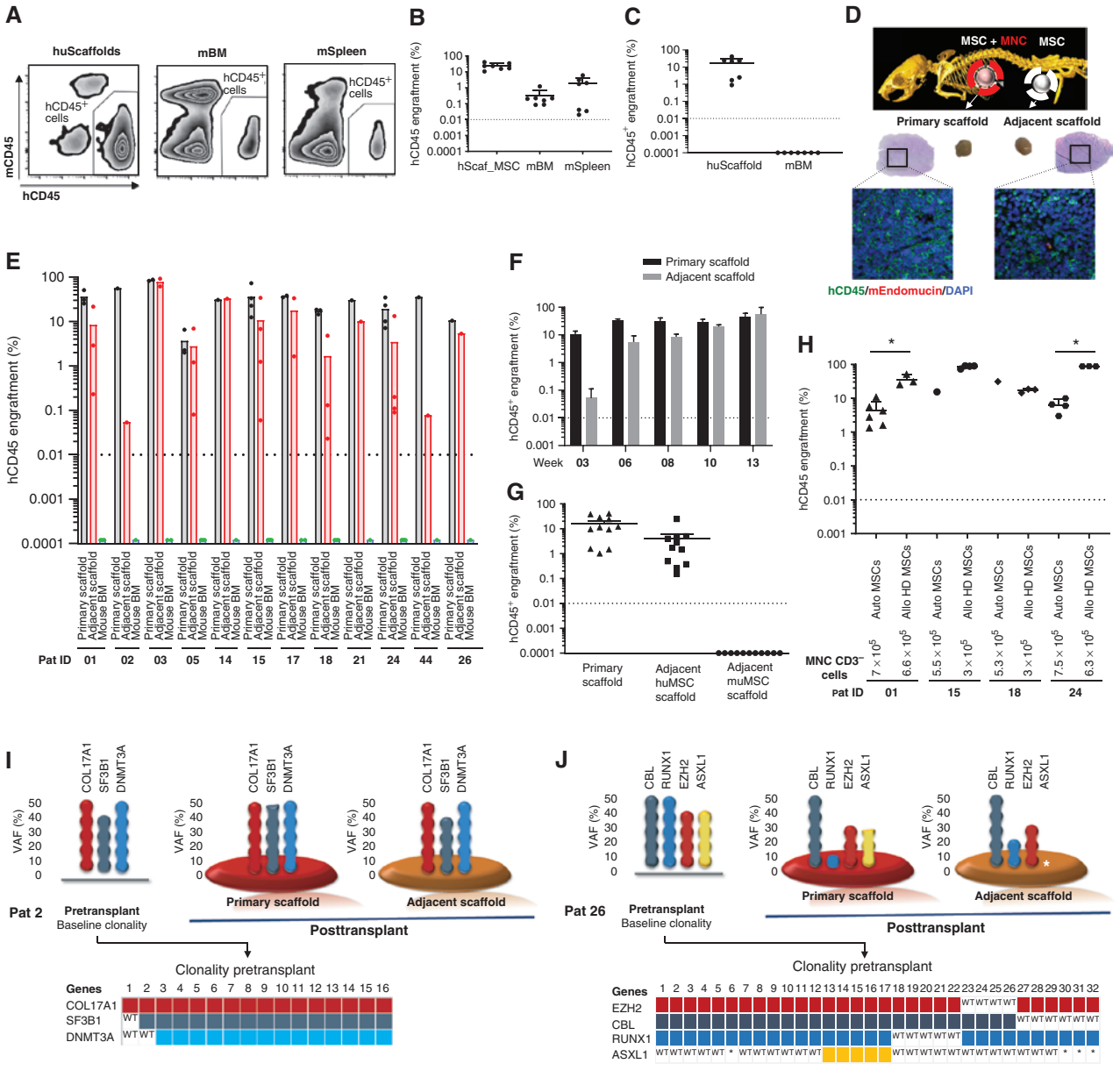

Figure 4. MDS HSPCs are highly dependent on the human MSC niche. **A,** Representative flow cytometry plot showing the engraftment of healthy hCD45+ cells in humanized niches, murine BM, and spleen in NSGW41 mice. **B,** Percentage of healthy donor hCD45+ cells in humanized niche, murine BM, and murine spleen in NSGW41 and/or NSG-SGM3 mice. **C,** Percentage of MDS hCD45+ cells in humanized scaffolds and murine BM in NSGW41 mice. **D,** Representative plot (immunofluorescence and hematoxylin and eosin staining) of the primary scaffold and adjacent scaffold after xenotransplantation in NSG-SGM3 mice. **E,** Percentage of total hCD45+ cells in primary scaffold, adjacent scaffold, and murine BM after xenotransplantation in NSG-SGM3 mice. **F,** *In vivo* migration kinetics of hCD45+ cells in the primary and adjacent scaffolds in NSG-SGM3 mice at various time points. **G,** Percentage of MDS hCD45+ cells in the humanized primary niche, adjacent niche with human MSCs, and adjacent niche with murine MSCs in NSG-SGM3 mice. **H,** Percentage of total hCD45+ cells in the humanized scaffolds that were seeded either with autologous (auto) MDS MSCs or allogenic healthy donor (allo HD) MSCs. Mice were kept alive for up to 18 weeks. **I** and **J,** Clonal distribution of patients with MDS in the primary pretransplanted HSPCs and primary and adjacent scaffolds following xenotransplantation. Bottom part of each figure shows the clonal spectrum at single-cell level (single-cell clonogenic assay) of primary day 0 pretransplanted HSPCs for each patient. **A–H,** Mice were injected with CD3− MNCs. huMSC, human MSCs; huScaffold, humanized scaffold; mBM, mouse BM; mSpleen, mouse spleen; muMSC, murine MSCs; Pat, patient; VAF, variant allele frequency; WT, wild-type. *, $P < 0.05$.

HSCs have no advantage, thus enabling engraftment of human HSPCs without myeloablative irradiation. We first used NSGW41 and NSG-SGM3 immunodeficient mice to test if BM cells from healthy adult individuals ($n = 6$ adult donors) can engraft in the humanized scaffolds and whether these cells can both migrate and colonize murine hematopoietic tissues. Following xenotransplantation, healthy adult donor HSPCs injected into the humanized scaffolds were able to engraft not only in the humanized niches but also in the murine BM and spleen at 12 weeks (Fig. 4A and B). The migratory behavior of healthy stem cells has been reported previously in healthy animals and humans (23–25).

In contrast, transplantation of MDS HSPCs in NSGW41 mice yielded hCD45$^+$ cell engraftment only in the humanized scaffolds (Fig. 4C). This behavior of MDS HSPCs led us to design an experiment to assess whether the MDS-SCs were unable to migrate through the vasculature or specifically failed in colonizing the murine hematopoietic tissues. In addition to the primary humanized scaffold containing MDS HSPCs, we implanted an adjacent MSC-seeded "empty scaffold" to provide an uncolonized humanized niche in NSG-SGM3 or NSGW41 mice (Fig. 4D). Following xenotransplantation, hCD45$^+$ engraftment was quantified in the primary scaffold and adjacent human MSC–seeded but not the murine BM. Our data clearly demonstrate that MDS HSPCs do migrate out of the primary scaffold and colonize the adjacent humanized scaffolds (Fig. 4D and E; Supplementary Fig. S3B–S3E). It is noteworthy that human hematopoietic cells start migrating from primary to adjacent scaffold as early as week 3 (Fig. 4F), before reaching a plateau at weeks 10 to 13. This migratory property of MDS-SCs was observed in all the cases studied here irrespective of the disease risk groups. Migration of the MDS-SCs occurred regardless of the location or distance between the primary and adjacent scaffolds. Notably, when NSG-SGM3 murine MSCs were used in adjacent scaffolds along with human MSCs in another adjacent scaffold, MDS HSPCs substantially migrated and homed only in the adjacent niche with human MSCs and not in the adjacent niche seeded with murine MSCs (Fig. 4G). This suggests that in the more permissive NSGW41 mouse model, healthy donor HSPCs can more or less equally compete with murine counterparts in the murine niche; however, this potent fitness is lacking in MDS HSPCs. Altogether, our data demonstrate that human MDS-SCs are entirely dependent on a humanized microenvironment to home and reconstitute, therefore implying a cross-talk between the MDS-SCs and the humanized niche–supporting cells (in this case human MSCs) that may be critical for establishment and progression of the disease.

Healthy Donor MSCs Could Also Provide Niche Support for MDS-SCs

Emerging evidence from our data and others suggests that there are functional deficits in the proliferation and differentiation of MDS MSCs (18). It is also becoming increasingly clear that alterations in the aging BM microenvironment can induce changes in hematopoiesis and that this effect may be exacerbated among MDS BM components due to the dysregulated inflammatory microenvironment (26–28). This led us to assess whether MSCs derived from the BM of patients with MDS are best to provide support to malignant HSPCs. Therefore, we compared the supportive capabilities of autologous MSCs (four patients) with allogenic healthy donor MSCs using our humanized scaffold system in NSG-SGM3 mice. Both types of scaffolds were seeded with the same number of MSCs ($\approx 5 \times 10^5$ cells per scaffold), and similar numbers of MDS HSPCs were injected into all of these scaffolds. Notably, the engraftment of MDS CD45$^+$ cells was similar and, in three out of four cases, even higher in mice that were implanted with scaffolds seeded with healthy donor MSCs (Fig. 4H). In patient 01, engraftment of hCD45$^+$ cells increased from 4.4% (in autologous-seeded MSCs) to 35.9% (in healthy donor–seeded MSCs). In patient 24, this increase was significantly higher—from 6.9% (in autologous-seeded MSCs) to 88.7% (in healthy donor–seeded MSCs). Our data suggest that MSCs derived from healthy donors are functionally able to support MDS-SCs, possibly even better than autologous MDS MSCs. Given the importance of this preliminary observation, further studies with larger patient cohorts and investigation of the clonal distribution in the engrafted cells are needed to confirm this behavior.

MDS HSPC Clones Migrate between the Humanized Niches

Having observed the migratory behavior of MDS HSPCs in *in vivo* humanized scaffolds, we next studied the clonal composition of the cells from the primary scaffold and those cells that had migrated into the adjacent scaffold. DNA sequencing analysis of the xenografted cells revealed that the mutant clones that migrate to the adjacent scaffolds are genetically similar (Fig. 4I and J; Supplementary Fig. S3F; Supplementary Table S4). For example, the clonality of the engrafted HSPCs in patient 02 was maintained in both primary and adjacent scaffolds (Fig. 4I). Interestingly, this patient had comparatively few subclones in the pretransplanted BM HSPCs at day 0 (Fig. 4I). In contrast, a multiclonal pattern was seen in the BM HSPCs of patient 26 prior to xenotransplantation (day 0; Fig. 4J). Our single-cell clonogenic assay revealed that at day 0, BM HSPCs from patient 26 had multiple subclones with *EZH2* as the founding mutation, whereas the other gene aberrations were acquired in a sequential order (Fig. 4J). Interestingly, a clonal fluctuation within the HSPCs was observed in the engrafted cells in the primary scaffolds. On the other hand, HSPC clones that had migrated into the adjacent scaffold lacked *ASXL1* mutations that were detected in both the primary scaffold and day 0 HSPCs. These data demonstrate the migratory behavior of malignant HSPCs and of potential differential motility behavior in *in vivo* settings of some subclones.

DISCUSSION

Understanding the biology of MDS-SCs and their interaction with the BM microenvironment remains a major challenge due to the lack of reliable *in vivo* disease models, thereby impeding translational MDS research. Here, for the first time, we provide an *in vivo* modeling approach to create a humanized microenvironment for MDS-SCs. These humanized scaffolds act as a framework to support cell proliferation and differentiation, and maintain not only the primary cellular phenotype and function but also the dysplastic morphology typically observed in MDS BM and blood. MSCs derived from patients with MDS were essential to create a stromal layer on the carrier biomaterial (or humanized scaffold) that acts as an "HSPC supportive niche" when the scaffolds are implanted into immunodeficient mice. These extramedullary humanized niches supported both human normal and malignant hematopoietic cells. Using high-resolution ultrasound imaging, we were able to show that these biometric scaffolds are vascularized as well as fully perfused. Remarkably, this humanized scaffold approach enabled engraftment of HSCs from approximately 94% of the patients with MDS tested here, independent

of MDS subtypes. The disease/age-associated lineage skewing that is often observed clinically and in MDS mouse models (29–32) was also captured in this *in vivo* system, in which we observed a myeloid differentiation bias that was particularly pronounced in high-risk cases. We were also able to show that MDS-SCs engraft and remain in primary transplants. Using secondary transplantation assays, we were able to functionally demonstrate their self-renewal and differentiation capacity within the *in vivo* humanized niches, thereby proving their stem cell capability. Although the engraftment in some secondary recipients was relatively reduced compared with the corresponding primary transplants, this could be due to the intrinsic aging of the BM HSCs, as similar results have also been observed in normal-aged mouse HSCs elsewhere (19, 20). Furthermore, in the knock-in MISTRG mouse model, similar engraftment in secondary transplants for low-risk MDS cases has been reported (33). The heterogeneity present among patients with MDS is also reflected in engraftment levels in our secondary transplants. Given the robustness of our scaffold-based system in generating primary as well as secondary transplants, it will be interesting to test more samples and also evaluate our scaffold model in the MISTRG mouse knock-in strain, and investigate whether further humanization of our scaffolds via the use of human endothelial cells, for example, could further improve the maintenance of long-term self-renewing MDS-SCs. Our quantitative targeted mutational analysis demonstrated the maintenance of the mutations that were present in the pretransplanted cells, indicating that these humanized niches in immunodeficient mice retain the original subclonal architecture of the patients with MDS.

In normal healthy adults, HSCs continuously migrate between the BM and blood; as such, they are always available to exit circulation in order to fill empty BM HSC niches (23, 25). Our data also demonstrate that HSPCs from healthy individuals migrated from human to human niche as well as to the murine hematopoietic niches. This behavior was not seen in MDS-SCs. Interestingly, MDS-SCs were able to migrate out of the primary niche but were subsequently homing and engrafting only in niches seeded with human MSCs. This preferential human niche requirement was observed even when these mice were maintained for 6 months after implantation of scaffolds. The preferential migratory behavior of primary MDS malignant stem cells in this *in vivo* setting is consistent with some previous reports in AML and acute lymphoblastic leukemia (34, 35), and further studies are needed to understand the dynamics of the migration and if this is associated with more aggressive MDS-SC properties. Our model provides a unique opportunity to study the clonal behavior of the cancers in general and to understand how these cancerous cells interact with different types of niches (e.g., healthy vs. malignant MSCs, young vs. aged MSCs, and role of endothelial cells).

It is becoming increasingly clear that alterations in the aging BM microenvironment can induce changes in hematopoiesis and that this effect may be exacerbated among MDS BM components due to the dysregulated inflammatory microenvironment (26–28). The change in the MDS microenvironment was noticeable from our *in vivo* data, as the alternative niche provided by healthy donor MSCs seems to enhance engraftment of MDS-SCs. This indicates the existence of a "dysplasia-like" defect in MDS MSCs, which are abnormal compared with their healthy counterparts but still provide enough support for the maintenance of the disease. Further studies are needed to confirm these preliminary findings.

Altogether, we believe that this new *in vivo* model is going to be critical for future investigations of the pathogenesis of MDS. It provides a robust preclinical system that will enable the development of new approaches for the treatment of MDS disease. Targeting the HSC–niche-specific interactions might not only prevent disease progression from precursor states such as ARCH and from MDS to AML, but will also enhance the effectiveness of current therapies directed at the malignant cells in a humanized microenvironment. Future functional studies are required to explore the receptor–ligand interacting signaling networks that may be essential for the MDS HSPC–niche interactions. In general, this will ultimately lead to the identification of rational therapeutic targets and the development of optimal strategies for intervention.

METHODS

Patient Samples

Patient samples ($n = 37$) were received from King's College London Haemato-Oncology Tissue Bank under research ethics protocol 08/H0906/94. Patient demographic and clinical characteristics are detailed in Supplementary Table S2. The clinical variables for all patients were ascertained at the time of sample collection. WES data were available for 25 patients, and myeloid-associated gene panel data were available for 2 patients (Supplementary Tables S1–S3).

Targeted DNA Mutation Sequencing

Targeted mutational analysis was performed on xenografted cells retrieved from the mice as previously described (3). PCR primers for patient-specific mutations were designed using Primer3 (RRID:SCR_003139) program (36,37). Here, PCR-amplified amplicons were normalized, mixed, and then processed using transposon-based Nextera XT technology (Illumina; Cat FC-131–1096, Cat FC-131–2001). Libraries were sequenced on the Illumina MiSeq platform. VCF and BAM data files were visualized using variant studio (Illumina) and integrated genome viewer (RRID:SCR_011793), respectively.

MNC, $CD34^+$, and $CD3^-$ Isolation from Human BM Cells

MNCs were isolated from BM cells by centrifugation using Ficoll-Paque PLUS (GE Healthcare Life Sciences). $CD3^-$ and/or $CD34^+$ cells enrichment was performed using the Easysep Human CD3 Positive Selection Kit (StemCell Technologies, Cat 18051) and Easysep Human CD34 Positive Selection Kit (StemCell Technologies, Cat 18056), respectively, along with Easysep magnet (StemCell Technologies, Cat 18000) according to the manufacturer's instructions.

Human MSC Expansion

Human BM MNCs were used for CD45 selection. CD45 selection was performed using Easysep Human CD45 Positive Selection Kit (StemCell Technologies, Cat 18259) and Easysep magnet (StemCell Technologies, Cat 18000) according to the manufacturer's instructions. $CD45^-$ cells were seeded at a density of $1 \times 10^6/cm^2$/0.2 to 0.3 mL of MSC culture media [MEM Alpha Medium (1X) + GlutaMAX-1 (Gibco, Cat 32571–029), 1% penicillin/streptomycin (Sigma-Aldrich, Cat P4333), and 10% human MSC-FBS (Gibco, Cat 12662–029)]. Cell culture media were removed and replenished 24 hours after seeding, and then once every week. Expanded MSCs were frozen as viable cells at passage 1 or 2.

Mouse Models

NOD/SCID/*IL2rγ*$^{-/-}$ (NSG, RRID:IMSR_JAX:005557) mice and NOD/SCID/*IL2rγ*$^{-/-}$/*IL3*/*GM*/*SF* (NSG-SGM3, RRID:IMSR_JAX:

013062) mice were originally obtained from Leonard Shultz (The Jackson Laboratory). NOD/SCID/*IL2rγ*$^{-/-}$/*Tyr*$^{+}$/*Kit* W41J (NBSGW, RRID:IMSR_JAX:026622) mice were purchased from The Jackson Laboratory. All three strains of mice (male/female) ages between 8 and 12 weeks used in this study were bred at The Francis Crick Institute Biological Research Facility. All animal experiments were performed at The Francis Crick Institute in accordance with UK Home Office and Crick guidelines and were undertaken under the Home Office project license PLL 70/8904.

Mouse MSC Expansion

NSG-SGM3 mice (age, up to 4 weeks; RRID:IMSR_JAX:013062) were sacrificed, and bones (femurs, tibias, and pelvis) were recovered. Mouse bones were cut longitudinally and then placed (inner BM tissue facing downward) onto the surface of a 10 cm culture dish. Culture dish was incubated for 10 minutes at room temperature. Note that 10 mL of mouse MSC media (MesenCult Expansion Kit, StemCell Technologies, Cat 05514; 1% penicillin/streptomycin, Sigma-Aldrich, Cat P4333) was added to the culture dish. After 3 days, media were collected and centrifuged at 300 × *g* for 6 minutes. Culture dish with mouse bones attached was washed 3 times with PBS without disturbing the bones. Fresh mouse MSC media (mixed with conditioned media, ratio 1:4) was added to the culture dish. At day 14, attached bones were removed using sterile forceps. Seventy-five percent of the media was replaced every week with fresh mouse MSC media. Cells were frozen at passage 1 and used later for *in vivo* experiments.

Cell Seeding of Scaffolds

All procedures were done in sterile conditions in a Class II biological safety cabinet. Human (and/or murine) MSCs were plated 7 to 10 days prior to seeding into the biometric scaffolds. Gelatin-based sponges (Gelfoam hemostatic agent absorbable gelatin sponge, Pfizer, Cat 00300090315085) were sectioned into 24 similar slices (6.6 mm × 7.5 mm × 7 mm), washed once with 70% ethanol and once with sterile PBS, and finally rehydrated with sterile PBS. MSCs (5×10^4–1×10^5, at passages 2–3) in 50 μL of respective MSC culture media were injected into each scaffold using a sterile insulin syringe. Seeded scaffolds were transferred to polystyrene ultralow attachment multiwell plate (Corning). Seeded scaffolds were incubated for up to 2 hours in a humidified cell culture incubator that was maintained at 37°C and 5% CO_2. Then MSC culture media were slowly added to the wells without disturbing scaffolds and incubated for an additional 48 hours.

CD3-depleted human BM MNCs (2.5×10^5 to 7.5×10^5) from patient or healthy donors were resuspended into MyeloCult H5100 (StemCell Technologies, Cat 05150, supplemented with 1% penicillin/streptomycin; Sigma-Aldrich, Cat P4333) supplemented with cytokines (20 ng/mL G-CSF, PeproTech, Cat 300–23; 20 ng/mL IL3, PeproTech, Cat 200–03; and 20 ng/mL TPO, PeproTech, Cat AF-300–18). CD3-depleted BM MNCs were then injected into the scaffolds that were preseeded with MSCs. For experiments where CD34^{+}CD38^{-} cells were injected into the scaffolds, 3×10^5 CD34^{-} accessory cells (irradiated 15 Gys) were also seeded alongside into each scaffold. Scaffolds were then incubated for up to 2 hours in a humidified cell culture incubator that was maintained at 37°C and 5% CO_2. Then MyeloCult H5100 (StemCell Technologies, Cat 05150, supplemented with 1% penicillin/streptomycin; Sigma-Aldrich, Cat P4333) supplemented with cytokines (20 ng/mL G-CSF, PeproTech, Cat 300–23; 20 ng/mL IL3, PeproTech, Cat 200–03; and 20 ng/mL TPO, PeproTech, Cat AF-300–18) was added slowly to the wells and incubated for an additional 24 hours.

Surgical Implantation of Preseeded Scaffold into Mice

Surgical implantation of the preseeded scaffolds was performed by following local-named veterinary surgeon guidelines for aseptic techniques. Mouse surgical area was prepared (shaved) 24 hours prior to the surgery. Note that 24 to 48 hours prior to the procedure, NSG and NSG-SGM3 mice received a sublethal dose of radiation (375cGy, where applicable) from a cesium-137 source. Mice were given analgesic (carprofen in drinking water, 0.1 mg/mL of water) 24 hours before the surgery. On the day of the surgery, mice were anesthetized in a chamber filled with 0.5% isoflurane and 2 L/min O_2. Analgesia [buprenorphine (0.1 mg/kg) and meloxicam (10 mg/kg)] was administered via the s.c. route. Then the skin around the surgical area was sterilized using 10% chlorhexidine solution with a clean swab. Note that 0.5 cm anterior-to-posterior incision of the skin was created, and then a pocket was made under the skin using sterile round-ended scissors (or forceps). Preseeded scaffold(s) were inserted into the incision, making sure it was placed deep within the pocket. Up to three preseeded (MSC^{+}CD3-depleted MNCs) scaffolds were implanted into each mouse. Scaffolds seeded with only MSCs were also implanted (when necessary). Incision site(s) were closed with surgical staples. Mice were maintained on analgesia (carprofen in drinking water, 0.1 mg/mL of water) for 48 hours after surgery. Surgical staples were removed 7 days after (no more than 10 days) the surgical procedure. Mice were administered with OTK3 (BioXCell, RRID:AB_1107632; ref. 38) via the intraperitoneal route on weekly basis for up to 4 weeks after surgery.

Engraftment was assessed in the scaffolds, BM (pooled femurs, tibias, and pelvis), and spleen at the time of sacrifice (12–18 weeks, or otherwise stated).

Hematoxylin and Eosin and Immunofluorescence of Biometric Scaffolds

Scaffolds retrieved from mice were fixed overnight in 10% neutral buffered formalin. Then scaffolds were processed, paraffin embedded, and sectioned (5 μm) for histologic analysis. Hematoxylin and eosin (H&E) staining was performed on the scaffolds. For immunofluorescence analysis, heat antigen retrieval was performed. Primary unconjugated antibodies used were specific for the following proteins: human CD45 (Agilent, RRID:AB_2314143) and Endomucin (Santa Cruz Biotechnology, RRID:AB_2100037). Secondary fluorescent antibodies (Invitrogen) were also used in this protocol. Images were captured using Zeiss Axio Scan Z1 slice scanner and Zen blue edition software.

Tissue Digestion

Scaffolds retrieved from mice were excised into small pieces and transferred into a 1.5 mL microcentrifuge tube that contained 1 mL of tissue digestion solution (Dispase, Sigma-Aldrich; 2 mg/mL Collagen Type I, StemCell Technologies, Cat 04902; 1 mg/mL DNase I, Sigma-Aldrich, Cat D4527–500KU; 10% FBS, Sigma-Aldrich). Tubes were incubated for up to a maximum of 1 hour in a water bath at 37°C. Digested cell suspension was filtered through a sterile 5 mL tube with a cell strainer cap. Cells were washed twice with washing buffer (PBS, 2% FBS and 1% penicillin/streptomycin).

Cell Sorting

BM cells from patients with MDS were stained with antibodies specific for human antigens (CD34 and CD38). DAPI (4,6, diamidino-2-phenylindole, Sigma-Aldrich, Cat D9542) staining was used to exclude dead cells and debris from the analysis. CD34^{+}CD38^{-} cells were FACS sorted and then used for injections into the scaffold preseeded with MSC, which were then used in *in vivo* experiments.

For xenografted cells, cells were stained with antibodies specific for human or murine antigens [mCD45: Thermo Fisher Scientific (RRID:AB_1107002); hCD45: Thermo Fisher Scientific (RRID:AB_1944375), Agilent (RRID:AB_2314143); hCD33: BD Biosciences (RRID:AB_395843, RRID:AB_398502), Thermo Fisher Scientific (RRID:AB_1907380); hCD19: Thermo Fisher Scientific (RRID:AB_1272053), BD Biosciences (RRID:AB_398597, RRID:AB_395812); hCD3: BD Biosciences

(RRID:AB_398591 RRID:AB_395740); hCD73: BD Biosciences (RRID:AB_2738063); hCD90: BD Biosciences (RRID:AB_2872219); hCD34: Thermo Fisher Scientific (RRID:AB_1963576), BD Biosciences, Cat 555824 (RRID:AB_398614, RRID:AB_2868843); and hCD38: Thermo Fisher Scientific (RRID:AB_2573346)]. DAPI or propidium iodide (PI; BD Biosciences, RRID:AB_2869075) staining was used to exclude dead cells and debris from the analysis. Cells were sorted as follows: myeloid cells (mCD45$^-$hCD45$^+$hCD33$^+$), lymphoid T cells (mCD45$^-$hCD45$^+$hCD3$^+$), lymphoid B cells (mCD45$^-$hCD45$^+$hCD19$^+$), and MSCs (mCD45$^-$hCD45$^-$hCD73$^+$hCD90$^+$).

Cell sorting was performed using a FACS Aria SORP (BD Biosciences). Sorted cells were washed in PBS and harvested in order to later perform further analysis (where needed).

Flow Cytometry Analysis

Following the tissue digestion of the scaffolds, xenografted cells were washed with PBS (2% FBS and 1% penicillin/streptomycin) and used for flow analysis. In addition, cells were recovered from the bones (femurs, tibias, and pelvis) and spleen of these mice. Cells were stained with antibodies specific for human or murine antigens [mCD45: Thermo Fisher Scientific (RRID:AB_1107002); hCD45: Thermo Fisher Scientific (RRID:AB_1944375), Agilent (RRID:AB_2314143); hCD33: BD Biosciences (RRID:AB_395843, RRID:AB_398502), Thermo Fisher Scientific (RRID:AB_1907380); hCD19: Thermo Fisher Scientific (RRID:AB_1272053), BD Biosciences (RRID:AB_398597, RRID:AB_395812); hCD3: BD Biosciences (RRID:AB_398591, RRID:AB_395740); hCD73: BD Biosciences (RRID:AB_2738063); hCD90: BD Biosciences (RRID:AB_2872219); hCD34: Thermo Fisher Scientific (RRID:AB_1963576), BD Biosciences, Cat 555824 (RRID:AB_398614, RRID:AB_2868843); and hCD38: Thermo Fisher Scientific (RRID:AB_2573346)]. DAPI or PI (BD Biosciences RRID: AB_2869075) staining was used to exclude dead cells and debris from the analysis. Cells were immunophenotyped by using Fortessa flow cytometer (BD Biosciences). Human myeloid cells, lymphoid B and T cells, and MSCs were detected as depicted in flow cytometry plot (Fig. 1C).

In Vivo *High-Resolution Ultrasound Perfusion Imaging of the Humanized Scaffolds*

To assess the blood perfusion of the humanized scaffolds, nonlinear contrast-enhanced ultrasound imaging was performed using a Vevo 3100 system with a MX550D transducer (VisualSonics) and Vevo MicroMarker nontargeted contrast agent (VisualSonics). The contrast agent was reconstituted according to the manufacturer's protocol at a concentration of 2×10^9 microbubbles/mL. Regular b-mode ultrasound imaging was used to position the imaging plane through the center of the scaffold before switching to nonlinear contrast mode. Mice were anesthetized in a chamber filled with 0.5% isoflurane and 2 L/min O_2. Imaging area around the implanted scaffold was shaved. While recording, a bolus injection of 50 μL contrast agent was administered via a tail vein catheter at a flow rate of 300 μL/min using a Vevo infusion pump (VisualSonics). Mice were maintained on 0.5% isoflurane and 2 L/min O_2 during the imaging process. At the end of the procedure, mice recovered to normality. Data analysis was performed using Vevo lab software (version 3.2.6, VisualSonics).

Colony-Forming Cell Assay

Five hundred primary BM CD34$^+$ HSPCs were plated in 0.5 mL in 24-well plate with MethoCult H4434 (StemCell Technologies, Cat 04434) supplemented with 1% penicillin/streptomycin (Sigma-Aldrich, Cat P4333). Assay was performed under hypoxic conditions (37°C and 3% O_2). After 14 days of culture, the numbers of colonies were counted and subsequently picked individually. Cells were washed with PBS and then frozen as cell pellet to be used for genomic sequencing analysis.

Genotyping of Colonies Derived from Single Cells

Single-cell colonies (colony-forming unit-granulocytes and macrophages and burst-forming unit-erythroid) were harvested at day 14 and washed twice with PBS. All single-cell–derived colonies were individually subjected to whole-genome amplification (GenomePlex Single Cell Whole Genome Amplification Kit, Sigma-Aldrich, Cat WGA4). Single-cell colonies were screened for patient-specific mutations. Gene mutation–specific amplicons were amplified through PCR using the primers as described in the "Targeted DNA Mutation Sequencing" section. All amplified libraries were subjected to Nextera XT (Illumina, Cat FC-131–1096, Cat FC-131–2001)–based library preparation and subsequently sequenced using MiSeq sequencing platform (Illumina).

Statistical Analysis

Prism Version 6 software (GraphPad, RRID:SCR_002798) was used for statistical analysis. Data are presented as the mean ± SEM (where applicable). Statistical analysis was performed using the unpaired *t* test for comparison of two groups to determine the level of significance. All the significant *P* values are described in the legends of the figures (where applicable).

Authors' Disclosures

G.J. Mufti reports personal fees from Novartis and grants from Bristol-Myers Squibb outside the submitted work. No disclosures were reported by the other authors.

Authors' Contributions

S.A. Mian: Conceptualization, data curation, formal analysis, investigation, visualization, methodology, writing–original draft, writing–review and editing. **A. Abarrategi:** Investigation, methodology. **K.L. Kong:** Formal analysis, investigation, methodology. **K. Rouault-Pierre:** Formal analysis, investigation, methodology, writing–review and editing. **H. Wood:** Resources, data curation, writing–review and editing. **C.A. Oedekoven:** Formal analysis, investigation, methodology. **A.E. Smith:** Data curation, formal analysis. **A. Batsivari:** Formal analysis, investigation, methodology. **L. Ariza-McNaughton:** Formal analysis, investigation, methodology. **P. Johnson:** Investigation, visualization, methodology. **T. Snoeks:** Investigation, visualization, methodology. **G.J. Mufti:** Supervision, funding acquisition, writing–review and editing. **D. Bonnet:** Conceptualization, supervision, funding acquisition, project administration, writing–review and editing.

Acknowledgments

The authors thank King's College London and King's College Hospital NHS Foundation Trust for funding the King's College London Haemato-Oncology Tissue Bank. They thank Rajani Chelliah for assisting with patient sample processing. They also thank the Biological Research Facility, Histopathology, In Vivo Imaging Facility, and the Flow Cytometry Core Facility teams at The Francis Crick Institute. This work was supported by The Francis Crick Institute, which receives its core funding from Cancer Research UK (FC001045), the UK Medical Research Council (FC001045), and the Wellcome Trust (FC001045) as well as the Blood Cancer UK program grant support (to King's College London and The Francis Crick Institute).

Received September 9, 2020; revised November 12, 2020; accepted December 18, 2020; published first December 23, 2020.

REFERENCES

1. Mufti GJ, Bennett JM, Goasguen J, Bain BJ, Baumann I, Brunning R, et al. Diagnosis and classification of myelodysplastic syndrome: International Working Group on Morphology of Myelodysplastic

Syndrome (IWGM-MDS) consensus proposals for the definition and enumeration of myeloblasts and ring sideroblasts. Haematologica 2008;93:1712–7.
2. Steensma DP. Myelodysplastic syndromes current treatment algorithm 2018. Blood Cancer J 2018;8:47.
3. Mian SA, Rouault-Pierre K, Smith AE, Seidl T, Pizzitola I, Kizilors A, et al. SF3B1 mutant MDS-initiating cells may arise from the haematopoietic stem cell compartment. Nat Commun 2015;6:10004.
4. Mian SA, Smith AE, Kulasekararaj AG, Kizilors A, Mohamedali AM, Lea NC, et al. Spliceosome mutations exhibit specific associations with epigenetic modifiers and proto-oncogenes mutated in myelodysplastic syndrome. Haematologica 2013;98:1058–66.
5. Haferlach T, Nagata Y, Grossmann V, Okuno Y, Bacher U, Nagae G, et al. Landscape of genetic lesions in 944 patients with myelodysplastic syndromes. Leukemia 2014;28:241–7.
6. Woll PS, Kjallquist U, Chowdhury O, Doolittle H, Wedge DC, Thongjuea S, et al. Myelodysplastic syndromes are propagated by rare and distinct human cancer stem cells in vivo. Cancer Cell 2014;25:794–808.
7. Medyouf H, Mossner M, Jann JC, Nolte F, Raffel S, Herrmann C, et al. Myelodysplastic cells in patients reprogram mesenchymal stromal cells to establish a transplantable stem cell niche disease unit. Cell Stem Cell 2014;14:824–37.
8. Rouault-Pierre K, Mian SA, Goulard M, Abarrategi A, Di Tulio A, Smith AE, et al. Preclinical modeling of myelodysplastic syndromes. Leukemia 2017;31:2702–8.
9. Krevvata M, Shan X, Zhou C, Dos Santos C, Habineza Ndikuyeze G, Secreto A, et al. Cytokines increase engraftment of human acute myeloid leukemia cells in immunocompromised mice but not engraftment of human myelodysplastic syndrome cells. Haematologica 2018;103:959–71.
10. Pang WW, Pluvinage JV, Price EA, Sridhar K, Arber DA, Greenberg PL, et al. Hematopoietic stem cell and progenitor cell mechanisms in myelodysplastic syndromes. Proc Natl Acad Sci U S A 2013;110:3011–6.
11. Benito AI, Bryant E, Loken MR, Sale GE, Nash RA, John Gass M, et al. NOD/SCID mice transplanted with marrow from patients with myelodysplastic syndrome (MDS) show long-term propagation of normal but not clonal human precursors. Leuk Res 2003;27:425–36.
12. Thanopoulou E, Cashman J, Kakagianne T, Eaves A, Zoumbos N, Eaves C. Engraftment of NOD/SCID-beta2 microglobulin null mice with multilineage neoplastic cells from patients with myelodysplastic syndrome. Blood 2004;103:4285–93.
13. Abarrategi A, Mian SA, Passaro D, Rouault-Pierre K, Grey W, Bonnet D. Modeling the human bone marrow niche in mice: from host bone marrow engraftment to bioengineering approaches. J Exp Med 2018;215:729–43.
14. Taussig DC, Vargaftig J, Miraki-Moud F, Griessinger E, Sharrock K, Luke T, et al. Leukemia-initiating cells from some acute myeloid leukemia patients with mutated nucleophosmin reside in the CD34(-) fraction. Blood 2010;115:1976–84.
15. Borgmann A, Baldy C, von Stackelberg A, Beyermann B, Fichtner I, Nurnberg P, et al. Childhood all blasts retain phenotypic and genotypic characteristics upon long-term serial passage in NOD/SCID mice. Pediatr Hematol Oncol 2000;17:635–50.
16. Rombouts WJ, Martens AC, Ploemacher RE. Identification of variables determining the engraftment potential of human acute myeloid leukemia in the immunodeficient NOD/SCID human chimera model. Leukemia 2000;14:889–97.
17. Nijmeijer BA, Mollevanger P, van Zelderen-Bhola SL, Kluin-Nelemans HC, Willemze R, Falkenburg JH. Monitoring of engraftment and progression of acute lymphoblastic leukemia in individual NOD/SCID mice. Exp Hematol 2001;29:322–9.
18. Geyh S, Oz S, Cadeddu RP, Frobel J, Bruckner B, Kundgen A, et al. Insufficient stromal support in MDS results from molecular and functional deficits of mesenchymal stromal cells. Leukemia 2013;27:1841–51.
19. Dykstra B, Olthof S, Schreuder J, Ritsema M, de Haan G. Clonal analysis reveals multiple functional defects of aged murine hematopoietic stem cells. J Exp Med 2011;208:2691–703.
20. Yamamoto R, Wilkinson AC, Ooehara J, Lan X, Lai CY, Nakauchi Y, et al. Large-scale clonal analysis resolves aging of the mouse hematopoietic stem cell compartment. Cell Stem Cell 2018;22:600–7.
21. Passaro D, Di Tullio A, Abarrategi A, Rouault-Pierre K, Foster K, Ariza-McNaughton L, et al. Increased vascular permeability in the bone marrow microenvironment contributes to disease progression and drug response in acute myeloid leukemia. Cancer Cell 2017;32:324–41.
22. Cosgun KN, Rahmig S, Mende N, Reinke S, Hauber I, Schafer C, et al. Kit regulates HSC engraftment across the human-mouse species barrier. Cell Stem Cell 2014;15:227–38.
23. Wright DE, Wagers AJ, Gulati AP, Johnson FL, Weissman IL. Physiological migration of hematopoietic stem and progenitor cells. Science 2001;294:1933–6.
24. Abkowitz JL, Robinson AE, Kale S, Long MW, Chen J. Mobilization of hematopoietic stem cells during homeostasis and after cytokine exposure. Blood 2003;102:1249–53.
25. Bixel MG, Kusumbe AP, Ramasamy SK, Sivaraj KK, Butz S, Vestweber D, et al. Flow dynamics and HSPC homing in bone marrow microvessels. Cell Rep 2017;18:1804–16.
26. Ganan-Gomez I, Wei Y, Starczynowski DT, Colla S, Yang H, Cabrero-Calvo M, et al. Deregulation of innate immune and inflammatory signaling in myelodysplastic syndromes. Leukemia 2015;29:1458–69.
27. Haas S, Hansson J, Klimmeck D, Loeffler D, Velten L, Uckelmann H, et al. Inflammation-induced emergency megakaryopoiesis driven by hematopoietic stem cell-like megakaryocyte progenitors. Cell Stem Cell 2015;17:422–34.
28. Zambetti NA, Ping Z, Chen S, Kenswil KJG, Mylona MA, Sanders MA, et al. Mesenchymal inflammation drives genotoxic stress in hematopoietic stem cells and predicts disease evolution in human pre-leukemia. Cell Stem Cell 2016;19:613–27.
29. Sun D, Luo M, Jeong M, Rodriguez B, Xia Z, Hannah R, et al. Epigenomic profiling of young and aged HSCs reveals concerted changes during aging that reinforce self-renewal. Cell Stem Cell 2014;14:673–88.
30. Challen GA, Sun D, Mayle A, Jeong M, Luo M, Rodriguez B, et al. Dnmt3a and Dnmt3b have overlapping and distinct functions in hematopoietic stem cells. Cell Stem Cell 2014;15:350–64.
31. Moran-Crusio K, Reavie L, Shih A, Abdel-Wahab O, Ndiaye-Lobry D, Lobry C, et al. Tet2 loss leads to increased hematopoietic stem cell self-renewal and myeloid transformation. Cancer Cell 2011;20:11–24.
32. Balderman SR, Li AJ, Hoffman CM, Frisch BJ, Goodman AN, LaMere MW, et al. Targeting of the bone marrow microenvironment improves outcome in a murine model of myelodysplastic syndrome. Blood 2016;127:616–25.
33. Song Y, Rongvaux A, Taylor A, Jiang T, Tebaldi T, Balasubramanian K, et al. A highly efficient and faithful MDS patient-derived xenotransplantation model for pre-clinical studies. Nat Commun 2019;10:366.
34. Antonelli A, Noort WA, Jaques J, de Boer B, de Jong-Korlaar R, Brouwers-Vos AZ, et al. Establishing human leukemia xenograft mouse models by implanting human bone marrow-like scaffold-based niches. Blood 2016;128:2949–59.
35. Reinisch A, Thomas D, Corces MR, Zhang X, Gratzinger D, Hong WJ, et al. A humanized bone marrow ossicle xenotransplantation model enables improved engraftment of healthy and leukemic human hematopoietic cells. Nat Med 2016;22:812–21.
36. Untergasser A, Cutcutache I, Koressaar T, Ye J, Faircloth BC, Remm M, et al. Primer3–new capabilities and interfaces. Nucleic Acids Res 2012;40:e115.
37. Koressaar T, Lepamets M, Kaplinski L, Raime K, Andreson R, Remm M. Primer3_masker: integrating masking of template sequence with primer design software. Bioinformatics 2018;34:1937–8.
38. Wunderlich M, Brooks RA, Panchal R, Rhyasen GW, Danet-Desnoyers G, Mulloy JC. OKT3 prevents xenogeneic GVHD and allows reliable xenograft initiation from unfractionated human hematopoietic tissues. Blood 2014;123:e134–44.